BORAY: A ray tracing code for various magnetized plasma configurations

BORAY: An Axisymmetric Ray Tracing Code Supports Both Closed and Open Field Lines Plasmas

Hua-sheng XIE[a,b], Banerjee Debabrata[a,b], Yu-kun BAI[a,b], Han-yue ZHAO[a,b], Jing-chun LI[c]

[a]*Hebei Key Laboratory of Compact Fusion, Langfang 065001, China*
[b]*ENN Science and Technology Development Co., Ltd., Langfang 065001, China*
[c]*Department of Earth and Space Sciences, Southern University of Science and Technology, Shenzhen, China*

Abstract

Ray tracing codes are useful to study the electromagnetic wave propagation and absorption in the geometrical optics approximation. In magnetized fusion plasma community, most ray tracing codes assume the plasma density and temperature be functions of the magnetic flux and study only the wave inside the last closed flux surface, which are sufficient for the present day tokamak. However, they are difficult to be used for configurations with open magnetic field line plasmas, such as mirror machine and field-reversed-configuration (FRC). We develop a ray tracing code in cylinder coordinates (r, ϕ, z) to support arbitrary axisymmetric configurations with both closed and open field lines plasmas. For wave propagation, the cold plasma dispersion relation is usually sufficient, and we require the magnetic field $\boldsymbol{B}(r, z)$ and species densities $n_{s0}(r, z)$ as input profiles. For wave absorption, we require a further temperature $T_{s0}(r, z)$ profile to solve a hot kinetic plasma dispersion relation. Different from other ray tracing codes which calculate the imaginary part of wave vector $\boldsymbol{k}_{\perp,i}$ for wave absorption, we calculate the imaginary part of wave frequency ω_i, which are shown to be equivalent under weak damping approximation. Both flexible numerical and analytical equilibria can be used. Examples and benchmarks with electron cyclotron wave, low hybrid wave and ion cyclotron wave for tokamak, spherical tokamak (ST), FRC and mirror machine are shown.

Keywords: Plasma waves, Ray tracing, Cold plasma dispersion relation, Kinetic plasma dispersion relation, Open field line plasmas

PROGRAM SUMMARY

Program Title: BORAY
Licensing provisions: BSD 3-clause
Programming language: Matlab
Nature of problem: Solve the plasmas electromagnetic wave propagation and absorption in the geometrical optics approximation for magnetized plasmas based on ray tracing of plasma dispersion relation. Based on axisymmetric (r, z) coordinates, the code can be used for many either closed field or open field lines plasmas configurations such as tokamak, spherical tokamak, FRC and mirror machine.
Solution method: Runge-Kutta time integral of ray tracing equations for wave propagation, and integral the imaginary part of the wave frequency in hot kinetic dispersion relation for wave absorption.
Additional comments including Restrictions and Unusual features (approx. 50-250 words): Kinetic relativistic effects are not included in the present version yet. Only axisymmetric two-dimensional (2D) profiles are support in present version.

Email address: huashengxie@gmail.com, xiehuasheng@enn.cn (Hua-sheng XIE)

1. Introduction

In magnetized confinement plasmas, waves heating is one of the most important approach to heating the plasma to high temperature (>10keV). The usually used waves from high frequency (~100GHz) to low frequency (<1MHz) include electron cyclotron wave (ECW), low hybrid wave (LHW), ion cyclotron wave (ICW) and Alfvén wave (AW). They would also have names such as fast wave (FW), slow wave (SW), helicon wave, etc. A simple but still accurate way to study the wave propagation and heating is using the geometrical optics approximation, which yields the ray tracing equations.

The ray tracing equations in Cartesian coordinates are

$$\frac{d\boldsymbol{r}}{dt} = \frac{\partial\omega}{\partial\boldsymbol{k}} = -\frac{\partial D/\partial\boldsymbol{k}}{\partial D/\partial\omega} = \boldsymbol{v}_g, \quad (1)$$

$$\frac{d\boldsymbol{k}}{dt} = -\frac{\partial\omega}{\partial\boldsymbol{r}} = \frac{\partial D/\partial\boldsymbol{r}}{\partial D/\partial\omega}, \quad (2)$$

with the dispersion relation

$$D(\omega, \boldsymbol{k}, \boldsymbol{r}) = 0, \quad (3)$$

where ray position $\boldsymbol{r} = (x, y, z)$ and wave vector $\boldsymbol{k} = (k_x, k_y, k_z)$. Here, ω is wave frequency, and $\boldsymbol{v}_g$ is wave group velocity.

Several widely used ray tracing codes have been developed in magnetic confinement fusion community, such as GENRAY[4], TORAY[6], C3PO[5], CURRAY[8] and TASK/WR[10]. However, most of them are developed for tokamak and use single fluid magnetohydrodynamics (MHD) equilibrium, thus the density and temperature profiles are set to be magnetic flux functions, and the open field line region is also omitted or simplified. To assume the density and temperature profiles be flux functions is helpful to obtain the flux average power absorption and to calculate the current driven. These treatments can be useful and sufficient for study the present day tokamak. However, they can not be used to the configurations with open field line plasmas or when the density and temperature are not magnetic flux functions. There are also codes for some special cases such as RAYS[7] (which is later updated to TORAY) for mirror configuration and FRTC[9] for LHW. In Ref.[15], a simplified model is used to study the ECRH in mirror. Thus, a code to remove these restrictions and can be used for wide situations would be useful, which motived the present work. The present work can be also seen as an extension version of the fluid and kinetic plasma dispersion relation solver BO code[1–3].

2. Equations to Solve

In this work, we use cylinder coordinates (r, ϕ, z). The wave vector variables are chosen as $(k_r, n_\phi = rk_\phi, k_z)$. The coordinates relations are $x = r\cos\phi$, $y = r\sin\phi$, $k_x = k_r\cos\phi - \frac{n_\phi}{r}\sin\phi$ and $k_y = k_r\sin\phi + \frac{n_\phi}{r}\cos\phi$. Note that the canonical coordinate for ϕ is n_ϕ, not k_ϕ. If we use k_ϕ as a coordinate, the ray tracing equation expressions would be more complicated, c.f., Ref.[11].

2.1. Ray tracing equations in cylinder coordinates

Do the coordinates transformation from (x, y, z, k_x, k_y, k_z) to $(r, \phi, z, k_r, n_\phi, k_z)$, we can have

$$\frac{dr}{d\tau} = \frac{\partial D}{\partial k_r}, \ \frac{d\phi}{d\tau} = \frac{\partial D}{\partial n_\phi}, \ \frac{dz}{d\tau} = \frac{\partial D}{\partial k_z}, \quad (4)$$

$$\frac{dk_r}{d\tau} = -\frac{\partial D}{\partial r}, \ \frac{dn_\phi}{d\tau} = -\frac{\partial D}{\partial \phi}, \ \frac{dk_z}{d\tau} = -\frac{\partial D}{\partial z}, \quad (5)$$

with

$$\frac{dt}{d\tau} = -\frac{\partial D}{\partial \omega}, \quad (6)$$

Usually, the dispersion relation (3) is written as $D = D(\omega, k_\parallel, k_\perp^2) = 0$. Here, the parallel wave vector $k_\parallel = \boldsymbol{k}\cdot\boldsymbol{b} = \frac{1}{B}\left(k_r B_r + k_z B_z + \frac{n_\phi}{r} B_\phi\right)$ is defined from the magnetic field $\boldsymbol{B}$, and $k_\perp^2 = k^2 - k_\parallel^2$, $B = B(r, z) = \sqrt{B_r^2 + B_z^2 + B_\phi^2}$, $k^2 = k_r^2 + k_z^2 + \frac{n_\phi^2}{r^2}$.

We only considered axisymmetric configurations, i.e., $\frac{\partial D}{\partial \phi} = 0$. We need to calculate the ray tracing equation from $(r, \phi, z, k_r, n_\phi, k_z)$ to $(r, \phi, z, k_\parallel^2, k_\perp^2, \alpha)$ with $\frac{\partial D}{\partial \alpha} = 0$, where α is the angle between two perpendicular wave vectors. We obtain

$$\frac{\partial D}{\partial k_r}\Big|_{r,\phi,z,n_\phi,k_z} = 2\Big(\frac{\partial D}{\partial k_\parallel^2} - \frac{\partial D}{\partial k_\perp^2}\Big)k_\parallel \frac{B_r}{B} + 2\frac{\partial D}{\partial k_\perp^2}k_r, \quad (7)$$

$$\frac{\partial D}{\partial n_\phi}\Big|_{r,\phi,z,k_r,k_z} = 2\Big(\frac{\partial D}{\partial k_\parallel^2} - \frac{\partial D}{\partial k_\perp^2}\Big)k_\parallel \frac{B_\phi}{rB} + 2\frac{\partial D}{\partial k_\perp^2}\frac{n_\phi}{r^2}, \quad (8)$$

$$\frac{\partial D}{\partial k_z}\Big|_{r,\phi,z,k_r,n_\phi} = 2\Big(\frac{\partial D}{\partial k_\parallel^2} - \frac{\partial D}{\partial k_\perp^2}\Big)k_\parallel \frac{B_z}{B} + 2\frac{\partial D}{\partial k_\perp^2}k_z, \quad (9)$$

$$\frac{\partial D}{\partial r}\Big|_{\phi,z,k_\parallel^2,k_\perp^2,\alpha} = \frac{\partial D}{\partial r}\Big|_{\phi,z,k_r,n_\phi,k_z} + 2\Big(\frac{\partial D}{\partial k_\parallel^2} - \frac{\partial D}{\partial k_\perp^2}\Big)k_\parallel \frac{\partial k_\parallel}{\partial r} - 2\frac{\partial D}{\partial k_\perp^2}\frac{n_\phi^3}{r^3} \quad (10)$$

$$\frac{\partial D}{\partial \phi}\Big|_{r,z,k_r,n_\phi,k_z} = 0, \quad (11)$$

$$\frac{\partial D}{\partial z}\Big|_{r,\phi,k_r,n_\phi,k_z} = \frac{\partial D}{\partial r}\Big|_{\phi,z,k_\parallel^2,k_\perp^2,\alpha} + 2\Big(\frac{\partial D}{\partial k_\parallel^2} - \frac{\partial D}{\partial k_\perp^2}\Big)k_\parallel \frac{\partial k_\parallel}{\partial z}, \quad (12)$$

where

$$\frac{\partial k_\parallel}{\partial r} = -\frac{k_\parallel}{B}\frac{\partial B}{\partial r} + \frac{1}{B}\Big(k_r\frac{\partial B_r}{\partial r} + k_z\frac{\partial B_z}{\partial r} + \frac{n_\phi}{r}\frac{\partial B_\phi}{\partial r} - \frac{B_\phi n_\phi}{r^2}\Big), \quad (13)$$

$$\frac{\partial k_\parallel}{\partial z} = -\frac{k_\parallel}{B}\frac{\partial B}{\partial z} + \frac{1}{B}\Big(k_r\frac{\partial B_r}{\partial z} + k_z\frac{\partial B_z}{\partial z} + \frac{n_\phi}{r}\frac{\partial B_\phi}{\partial z}\Big). \quad (14)$$

2.2. Ray tracing equations for cold plasma dispersion relation

Cold plasma dispersion relation

$$F(\omega, k_\parallel^2, k_\perp^2) = \varepsilon_1 \frac{k_\perp^4 c^4}{\omega^4} - \Big[(\varepsilon_1 + \varepsilon_3)\Big(\varepsilon_1 - \frac{k_\parallel^2 c^2}{\omega^2}\Big) - \varepsilon_2^2\Big] \frac{k_\perp^2 c^2}{\omega^2} + \varepsilon_3\Big[\Big(\varepsilon_1 - \frac{k_\parallel^2 c^2}{\omega^2}\Big)^2 - \varepsilon_2^2\Big] = 0, \quad (15)$$

where

$$\varepsilon_1 = 1 - \sum_s \frac{\omega_{ps}^2}{\omega^2 - \omega_{cs}^2}, \quad \varepsilon_2 = \sum_s \frac{\omega_{cs}}{\omega} \frac{\omega_{ps}^2}{\omega^2 - \omega_{cs}^2}, \quad \varepsilon_3 = 1 - \sum_s \frac{\omega_{ps}^2}{\omega^2}, \quad (16)$$

$$\boldsymbol{n} = \frac{\boldsymbol{k}c}{\omega}, \ \omega_{cs} = \frac{q_s B}{m_s}, \ \omega_{ps} = \sqrt{\frac{n_{s0} q_s^2}{\epsilon_0 m_s}}, \ \ c = \frac{1}{\sqrt{\mu_0 \epsilon_0}}. \quad (17)$$

The derivates expressions for F can be readily written out explicit, i.e., $\frac{\partial F}{\partial k_\parallel^2}$, $\frac{\partial F}{\partial k_\perp^2}$, $\frac{\partial F}{\partial r}\Big|_{\phi,z,k_\parallel^2,k_\perp^2,\alpha}$, $\frac{\partial F}{\partial z}\Big|_{r,\phi,k_\parallel^2,k_\perp^2,\alpha}$ and $\frac{\partial F}{\partial \omega}$.

We need the 2D equilibrium profiles $B_r(r,z)$, $B_z(r,z)$, $B_\phi(r,z)$, $B_(r,z)$, $n_{s0}(r,z)$ and their first order derivate $\partial/\partial r$ and $\partial/\partial z$.

We should note that the cold plasma dispersion relation Eq.(15) is singular at cyclotron resonant position of species $s = a$, say, if $\omega \simeq \omega_{c,s=a}$. This singularity is first order to $Y_a = 1 - \omega_{c,s=a}^2/\omega^2$, thus we can multiple Eq.(15) to define a new dispersion relation $G(\omega, k_\parallel^2, k_\perp^2) = Y_a F(\omega, k_\parallel^2, k_\perp^2)$ in the code, which is similar to the treatment in GENRAY[4]. We should also be careful that we should not use $G'(\omega, k_\parallel^2, k_\perp^2) = Y_a^n F(\omega, k_\parallel^2, k_\perp^2)$ ($n \geq 2$), which will cause the group velocity vanish at resonant position.

We can also see that the above equations have no limitations for whether the plasmas are in open field lines or in closed field lines. That is, the equations are the same for both cases.

2.3. Wave absorption equation using hot kinetic plasma dispersion relation

Since the drift bi-Maxwellian distribution function may lead unstable modes with imaginary part of wave frequency be positive, i.e., wave absorbs energy from particles, we only use the Maxwellian distribution hot kinetic dispersion relation for wave heating in the present version of BORAY. The non-relativistic dispersion tensor is standard, c.f., [2].

For weak damping approximation with $\omega_i \ll \omega_r$ and $\boldsymbol{k}_i \ll \boldsymbol{k}_r$, for $D(\omega, \boldsymbol{k}) = D_r(\omega, \boldsymbol{k}) + iD_i(\omega, \boldsymbol{k}) = 0$, $D_i \ll D_r$, we have $D_r(\omega_r, \boldsymbol{k}_r) = 0$ and

$$i\Big[\frac{\partial D_r(\omega_r, \boldsymbol{k}_r)}{\partial \omega_r}\omega_i + D_i(\omega_r, \boldsymbol{k}_r)\Big] \simeq 0, \quad (18)$$

$$i\Big[\frac{\partial D_r(\omega_r, \boldsymbol{k}_r)}{\partial \boldsymbol{k}_r}\boldsymbol{k}_i + D_i(\omega_r, \boldsymbol{k}_r)\Big] \simeq 0, \quad (19)$$

we have

$$\boldsymbol{k}_i = -\frac{D_i}{\partial D_r/\partial \boldsymbol{k}_r}, \ \ \omega_i = -\frac{D_i}{\partial D_r/\partial \omega_r}, \quad (20)$$

$$\boldsymbol{k}_i = \frac{\partial D_r/\partial \omega_r}{\partial D_r/\partial \boldsymbol{k}_r}\omega_i = -\frac{\omega_i}{\partial \omega/\partial \boldsymbol{k}_r} = -\frac{\omega_i}{\boldsymbol{v}_g}, \quad (21)$$

So the wave damping caused wave intensity $P(s)$ along the trajectory can be calculated from either $\boldsymbol{k}_i$ or ω_i, due to

$$P(s) = 1 - e^{-2\int_0^s \boldsymbol{k}_i \cdot d\boldsymbol{r}} = 1 - e^{-2\int_0^t \omega_i dt}.$$

One can use Eq.(20) to calculate ω_i when the weak damping assumption is valid. In BORAY, we choose to calculate the complex $\omega = \omega_r + i\omega_i$ more accurately along the ray, since that usually the kinetic ω_r may deviate from initial wave frequency ω_0. The BO code[1–3] is convenient to calculate the ω for given real $\boldsymbol{k}$ for either kinetic or fluid plasma dispersion relations. So, we inherit the corresponding modules of BO to calculate the kinetic absorption in the present ray tracing code. Hence, we named the present code as BO-RAY (or, BO-RAY) as a branch of BO family.

To calculate the absorption ratio from different species, we keep only the temperature of that species un-change and set the temperatures of other species be cold.

3. Benchmark and Applications

In this section, to show the correction and capability of BORAY, we compare it with other ray tracing code, particle simulation and experiments. If not specialized, the tokamak and ST equilibria in the following examples are obtained from EFIT[12] outputs of corresponding configurations. All the examples in this section are summarized in Table 1, which are obtained by BORAY under a unified theoretical model and numerical code as described in Sec.2, i.e., we do not need to choose different models for different examples. The only differences between different examples are the input magnetic fields, densities and temperatures profiles, and the initial wave frequency, position and wave vector.

Table 1: BORAY benchmark and application examples, for varies wave frequencies and varies configurations, with numerical MHD equilibria (default), 3-fluid equilibrium (Fig.8) and analytical MHD equilibrium (Fig.9).

Configuration (Field Lines) B_ϕ	Tokamak (Closed) $\neq 0$	ST (Both) $\neq 0$	FRC (Both) $= 0$	Mirror (Open) $= 0$
ECW (O&X)	Fig.1	Fig.8 (3-fluid eq.)		
LHW	Fig.2			Fig.6
Helicon	Fig.3			
HHFW			Fig.5	
ICW		Fig.4, Fig.9 (analy. eq.)		Fig.7

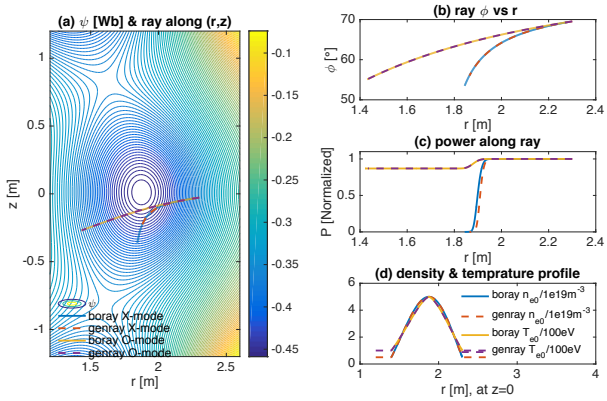

Figure 1: Comparison of BORAY and GENRAY for EAST tokamak 100GHz ECW O and X modes. Both ray trajectories and power absorptions agree well.

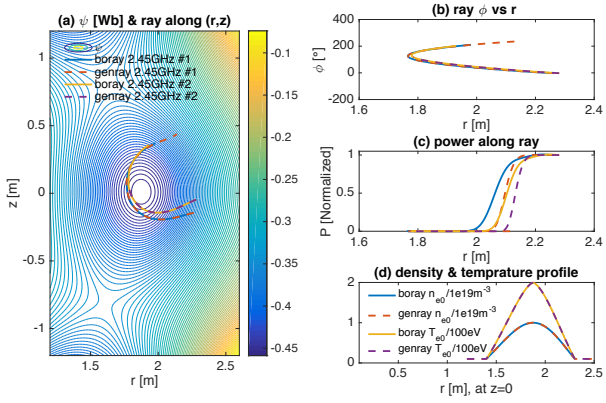

Figure 2: Comparison of BORAY and GENRAY for EAST tokamak 2.45GHz LHW. Ray trajectories agree well. However, GENRAY damping early than BORAY for power absorptions, which may due to different absorption models used in the two codes.

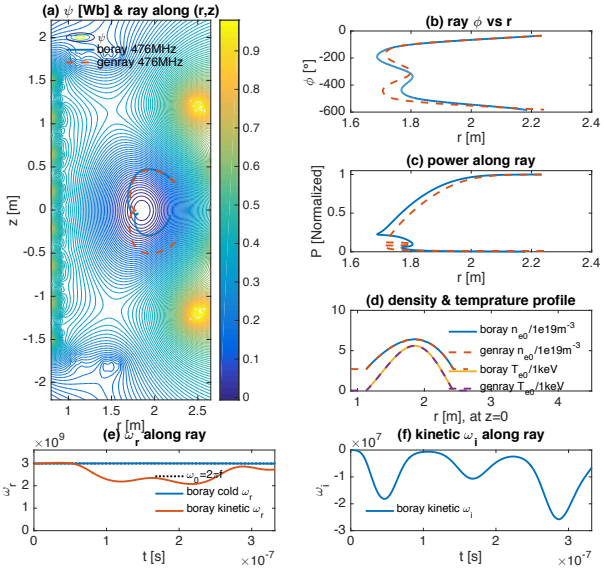

Figure 3: Comparison of BORAY and GENRAY for HL-2M tokamak 476MHz helicon wave[16]. Ray trajectories and power absorptions roughly agree. The difference may come from the numerical errors in GENRAY, since less than 200 points is used along the ray in GENRAY output.

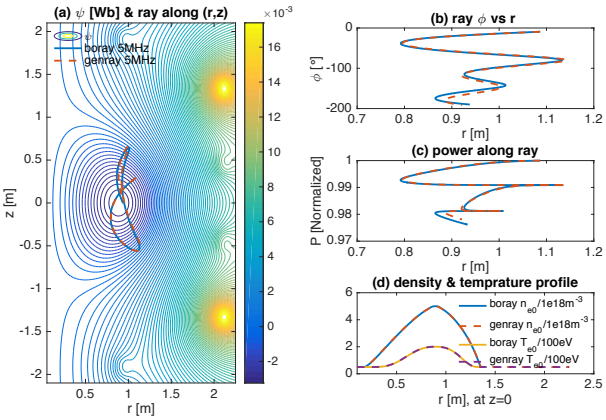

Figure 4: Comparison of BORAY and GENRAY for EXL-50 spherical tokamak 5MHz ICW. Both ray trajectories and power absorptions agree well. The slight difference may come from numerical error of time push or grid interpolation.

3.1. Tokamak and ST ECW, LHW and ICW

In this subsection, we show the benchmarks between BORAY and GENRAY for several standard tokamak and ST cases, including the frequency from high to low, i.e., ECW X-mode and O-mode, LHW, helicon wave, and ICW.

Fig.1 shows the comparison of BORAY and GENRAY for EAST tokamak ECW X-mode and O-mode, with central magnetic field $B_0 = 1.78T$, major radius $R_0 = 1.88m$, safety factor $q_0 = 1.5$, density $n_{e0} = 5 \times 10^{19} m^{-3}$ and temperature $T_{e0} = T_{i0} = 500eV$.

Fig.2 shows the comparison of BORAY and GENRAY for EAST tokamak 2.45GHz LHW for the same equilibrium magnetic fields as in Fig.1, but different densities and temperatures, $n_{e0} = 1 \times 10^{19} m^{-3}$ and $T_{e0} = T_{i0} = 200eV$.

Fig.3 shows the comparison of BORAY and GENRAY for HL-2M tokamak 476MHz helicon wave, with central magnetic field $B_0 = 1.76T$, major radius $R_0 = 1.85m$, safety factor $q_0 = 0.98$, density $n_{e0} = 6.42 \times 10^{19} m^{-3}$, $n_{D^+0} = 5.39 \times 10^{19} m^{-3}$, $n_{C^{+6}0} = 0.17 \times 10^{19} m^{-3}$ and temperature $T_{e0} = 5.60keV$, $T_{D^+0} = T_{C^{+6}0} = 4.78keV$.

Fig.4 shows the comparison of BORAY and GENRAY for EXL-50 spherical tokamak 5MHz ICW, with central magnetic field $B_0 = 0.26T$, major radius $R_0 = 0.89m$, safety factor $q_0 = 10.9$, density $n_{e0} = 5.0 \times 10^{18} m^{-3}$ and temperature $T_{e0} = 200eV$ and $T_{i0} = 50eV$.

In all these above benchmark cases, both ray trajectories and power absorptions agree well. Some differences may come from numerical error or slight different models in the two codes. We can do some analysis of how valid of the BORAY results. For example, in Fig.3(e), we show the ω_r along the ray, which are solved from the cold and kinetic dispersion relations with the ray tracing output $\boldsymbol{k}$ along the ray. We see that the cold plasma ω_r is almost identical to the given input wave frequency $\omega_0 = 2\pi f$, which means that the cold plasma ray tracing equation is solved accurately in BORAY. The deviate of kinetic ω_r to ω_0 implies that the cold plasma assumption for the ray tracing may not be accurate for this case. However, the $\omega_i/\omega_r \simeq 0.01$ means that the weak damping assumption still holds.

3.2. FRC High Harmonic Fast Wave

A major advantage between BORAY and most of other ray tracing codes is that BORAY can support both closed and open field lines plasmas naturally. We firstly show the result for FRC case. Fig.5 shows C2-U FRC 7MHz High Harmonic FW (HHFW) simulation results, which is similar to the GENRAY-C results in Ref.[13],

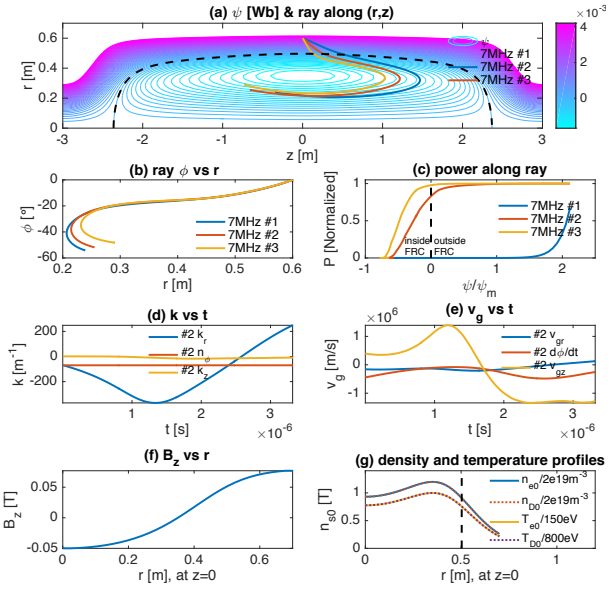

Figure 5: C2-U FRC 7MHz HHFW simulation results, which is similar to the results in Ref.[13], i.e., the absorption can be 100% and most power can be deposited inside the closed flux surface for optimized wave parameters.

i.e., the absorption can be 100% and most power can be deposited inside the closed flux surface for optimized wave parameters. The equilibrium is generated by GSEQ-FRC[14] using similar parameters as in Ref.[13], with axis magnetic field $B(0,0) = -0.05T$, major radius $R_0 = 0.35m$, central density $n_{e0} = 2.4 \times 10^{19} m^{-3}$ and temperature $T_{e0} = 150eV$ and $T_{D^+1 0} = 800eV$.

3.3. Mirror LHW and ICW

Here, we show the capability of BORAY for mirror configuration. Fig.6 shows mirror 160MHz LHW simulation results, which is close to the three dimensional (3D) particle-in-cell (PIC) simulations results in Ref.[17] as shown in Fig.6(b) for both the ray trajectories and turning points. Here, the initial antenna $k_z = 16.3m^{-1}$. Note that the density is given as $n_{s0} = n_0 e^{-\frac{r^2}{2\sigma^2}}$, which is not set as function of magnetic flux. Here, $n_0 = 1 \times 10^{18} m^{-3}$ and $\sigma = 0.045m$. Temperature is set as constant for both electrons and H ions, $T_{e0} = T_{H0} = 460eV$.

Fig.7 shows KMAX mirror 750kHz ICW simulation results, which is close to the results in Ref.[22] of ICRF experiment, i.e., absorption rate > 40%. Initial wave parameters $(r, \phi, z, k_{r,guess}, n_\phi, k_z) = (0.2, 0, 0.9, 90.2, -1, -8)$. Note that the summation of ion and electron damping rates is not equal to the total damping rate, which is probably due to the break of

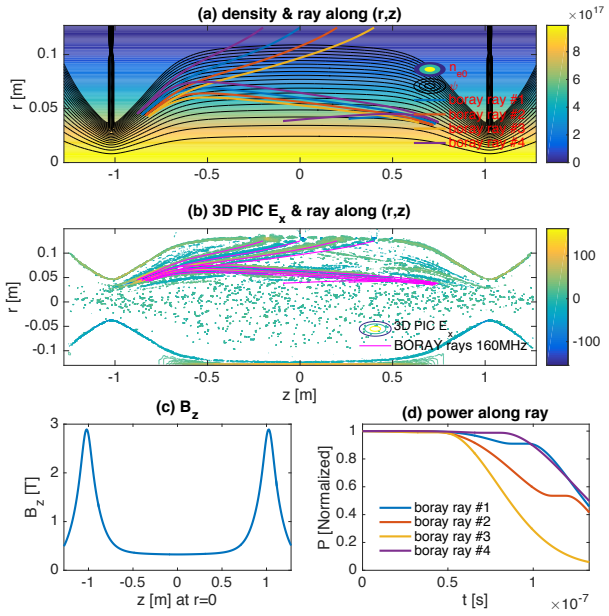

Figure 6: Mirror 160MHz LHW simulation results, which is close to the results in Ref.[17] of 3D PIC simulations (b), where the PIC data with $E_x < 10$ is removed to make the figure more clear. The power absorptions (d) are also similar, i.e., the wave is almost decayed away before reaching the second turning point.

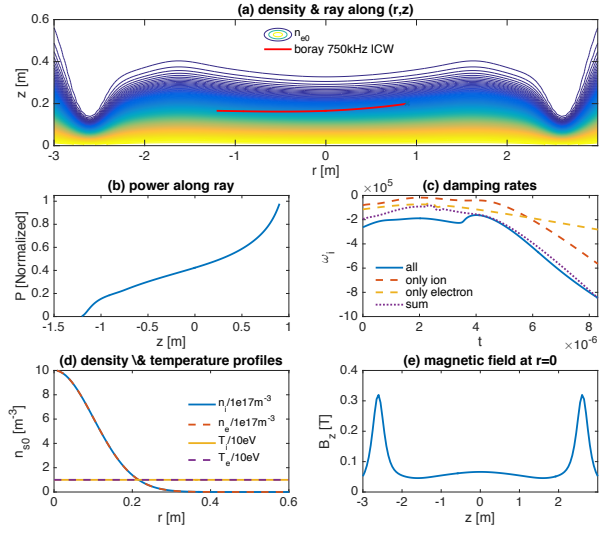

Figure 7: KMAX mirror 750kHz ICW simulation results, which is close to the results in Ref.[22] of ICRF experiment, i.e., absorption rate > 40%.

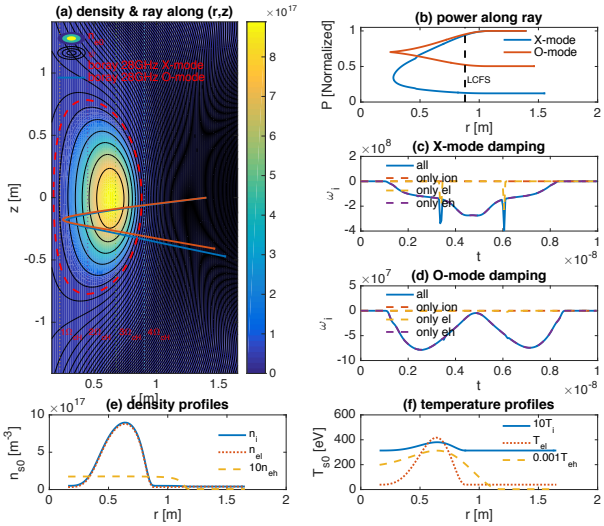

Figure 8: EXL-50 spherical tokamak 28GHz ECW O&X-modes, with three-fluid equilibrium. The high energy electrons (*eh*) contribute most of the power absorption, whereas the absorption from ions and low energy electrons (*el*) are negligible.

weak damping approximation or that the effects of different species are not independently.

3.4. ST ECW under multi-fluid equilibrium

In some STs, such as QUEST[19] and EXL-50[20], the high energy electrons (>10keV) are an important component. Ref.[18] provides a multi-fluid equilibrium model for EXL-50. Here, we show the capability of BORAY for this equilibrium configuration. Fig.8 shows the EXL-50 spherical tokamak 28GHz ECW O&X-modes under three-fluid equilibrium with central magnetic field $B_0 = 0.36T$, major radius $R_0 = 0.63m$, safety factor $q_0 \simeq 10$, maximum densities $n_{H^+} = 9.0 \times 10^{17} m^{-3}$, $n_{el} = 8.8 \times 10^{17} m^{-3}$, $n_{eh} = 1.76 \times 10^{16} m^{-3}$ and temperatures $T_{H^+} = 38eV$, $T_{el} = 417eV$ and $T_{eh} = 313keV$. The low density (~2%) high energy electrons (*eh*) contribute most of the power absorption, whereas the absorption from H^+ ions and low energy electrons (*el*) are negligible. We obtain the three fluid equilibrium profiles for both inside and outside the last closed flux surface (LCFS) from the model in Ref.[18] for EXL-50 shot#6935 t=4.45s, with total plasma current $I_p = 120kA$. We also see that the X-mode have better absorption than O-mode, and the second order $2\omega_{cH}$ resonant is also stronger than that of O-mode. These high energy electron effects are similar to the recently reported[21] QUEST experimental and theoretical analysis results. We can also see from Fig.8 (b) that some amount (~ 5%) of the wave absorption is outside the LCFS.

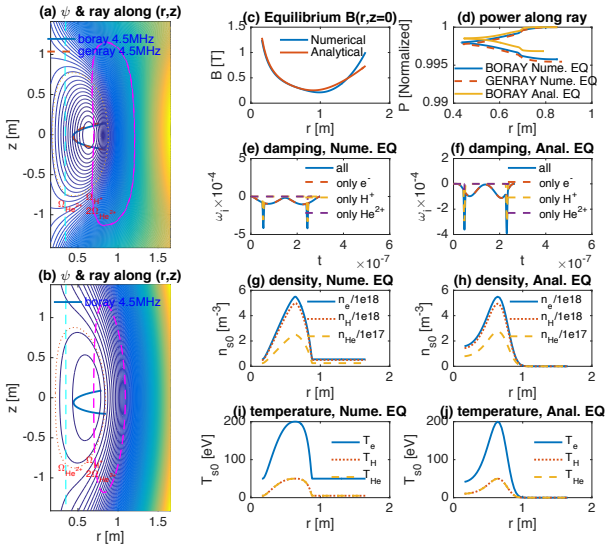

Figure 9: Comparison EXL-50 spherical tokamak 4.5MHz ICW for numerical and analytical MHD equilibria, with three species, i.e., electrons, H^+ ions and 5% He^{2+} minority ions. Both ray trajectories and power absorptions are similar.

3.5. Compare ST ICW under numerical and analytical equilibria

We are interested in how the differences can be for wave propagation and absorption between numerical and analytical equilibria. Fig.9 shows the comparison of EXL-50 spherical tokamak 4.5MHz ICW for numerical and analytical MHD equilibria, with three species, i.e., electrons, H^+ ions and 5% He^{2+} minority ions. The numerical equilibrium parameters are $B_0 = 0.32T$, major radius $R_0 = 0.64m$, safety factor $q_0 = 1.6$, density $n_{e0} = 5.5 \times 10^{18} m^{-3}$ and temperature $T_{e0} = 200eV$ and $T_{i0} = 50eV$. The construction of analytical equilibrium is described at Appendix B, with other model parameters $R_x = 0.17m$, $E = 1.5$, $\tau = 0.8$, $L_{ns} = 0.9$ and $L_{ts} = 0.8$ for the present case. Both ray trajectories and power absorptions are similar for the numerical and analytical equilibria. For both cases, the CPU runtimes of ray tracing are in seconds for 10000 points. The numerical equilibrium case (3s) is slightly faster than the analytical equilibrium case (7s). For this case, most power is absorbed by electrons and fundamental Ω_{cH^+} resonant, with also slight $2\Omega_{cHe^{2+}}$ resonant as can be seen from the damping rate sub-figures (e)&(f). This benchmark implies that the analytical equilibrium can be good enough to study the rough wave features of the actual devices.

4. Summary

A new plasma wave ray tracing code BORAY (https://github.com/hsxie/boray) has been developed for axisymmetric configurations to support both closed and open field lines plasmas configurations. The code shows good agreement with GENRAY code for tokamak and ST cases of ECW, LHW, helicon wave and ICW, and also agree well with 3D PIC simulation of LHW in mirror machine, and agree with GENRAY-C for HHFW in FRC, and ICW for KMAX mirror experiment. Thus, it can be expected that BORAY can have widely application for the plasma wave propagation and heating studies and especially to help the design of the wave heating system to choose the wave parameters. The code supports both numerical and analytical equilibria. Future works can include relativistic and collisional effects and calculating the current driven. Modified the cold plasma ray tracing model to kinetic dispersion relation to support electron and ion Bernstein waves could also be an important future topic.

Acknowledgments Discussion with Shao-dong Song, Guang-hui Zhu are acknowledged. We also thank Jiangshan Zheng for providing the 3D PIC mirror LHW simulation data, Wen-jun Liu for providing the three fluid equilibrium of EXL-50 spherical tokamak and Yu.V. Petrov and R.W. Harvey for the introduction of GENRAY code. This work is supported by the compact fusion project in ENN group.

Appendix A. More Details of BORAY

Bi-linear interpolation is used for uniform (r, z) grids, which can be fast, and even can be faster than analytical equilibrium if we calculated the interpolation coefficients beforehand. In many tests, we find it is accurate enough. For wave absorption, we do not need calculate every point along the ray. Instead, we calculated the ray trajectory firstly with high accuracy, say $\geq$ 10000 points, and then select several points, say 200-1000 points, to calculate the damping rates, and then integral them to obtain the power absorption. SI units are used for all variables, except that the temperature unit is eV.

The user should generate the initial magnetic fields, densities and temperatures profile firstly and also give their derivatives to r and z. Also, the user should give the initial wave parameters, i.e., wave frequency $f = \omega/2\pi$ and $(r, \phi, z, k_{r,guess}, n_\phi, k_z)$. To make $D(\omega, \boldsymbol{k}) = 0$, BORAY calculate k_r from given n_ϕ and k_z. Multi-k_r may

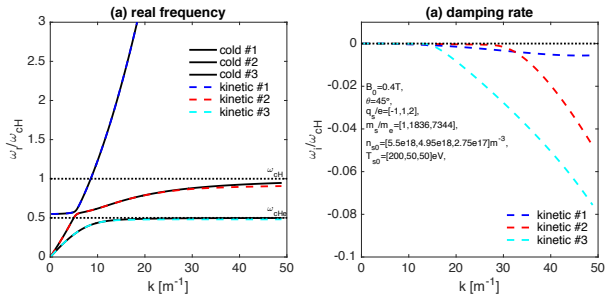

Figure A.10: Waves in ICW range for the EXL-50 He^{2+} minority ions heating case. Solutions are calculated by the fluid and kinetic versions of BO[1].

exist, the user can adjust $k_{r,guess}$ to solve the corresponding k_r who wants. For examples, we use different $k_{r,guess}$ to obtain X and O modes.

To analysis the wave feature in multi-species plasmas and to find the reasonable initial wave vector, the fluid and kinetic version of BO code can be useful, which can give all the wave frequency ω solutions for given wave vector $\boldsymbol{k}$ at one time without the requirement of initial guess frequency and thus will not miss solutions. We show a typical ω vs. k figure in Fig.A.10 for ICRF minority heating parameter relevant to the case in Fig.9. For this case, we can see that three branches exist in the ion cyclotron frequency range, and the kinetic correction to the cold plasma real frequency is small. Table A.2 summaries the role of each codes in BO family.

Table A.2: Fluid and kinetic plasma waves and instabilities code BO family[1–3].

	Type	Names	References
BO family (open source)	dispersion relation ($\boldsymbol{k} \to \omega$)	PDRF, PDRK, BO, BO2.0	Xie14, 16,19,21
	ray tracing ($\omega \to \boldsymbol{k}$)	BORAY	Xie21 (this work)

Appendix B. Analytical Solovév equilibrium for varies configurations

Analytical equilibrium can be useful for fast study the wave feature and can avoid the numerical interpolation error of numerical equilibrium from discrete grids. We construct an analytical Solovév equilibrium to include tokamak, spherical tokamak, FRC and mirror configuration in a same model, and which is also the solution of Grad-Shafranov MHD equilibrium equation.

The normalized equilibrium poloidal flux is[23]

$$\psi(r,z) = -RA_\phi = \frac{\psi_0}{R_0^4}\Big\{(R^2-R_0^2)^2 + \frac{Z^2}{E^2}(R^2-R_x^2) \quad \text{(B.1)}$$
$$-\tau R_0^2\Big[R^2 ln(\frac{R^2}{R_0^2}) - (R^2-R_0^2) - \frac{(R^2-R_0^2)^2}{2R_0^2}\Big]\Big\},$$

where R_0 is major radius and the magnetic axis position $\psi(R_0,0) = 0$. R_x, E and τ control the position of X-point, elongation and triangularity. The magnetic field are

$$B_r = -\frac{1}{r}\frac{\partial\psi}{\partial z} = -\frac{2\psi_0}{rR_0^2}\Big[\frac{Z}{E^2}(R^2-R_x^2)\Big], \quad \text{(B.2)}$$

$$B_z = \frac{1}{r}\frac{\partial\psi}{\partial r} = \frac{2\psi_0}{R_0^4}\Big\{2(R^2-R_0^2) + \frac{Z^2}{E^2} \quad \text{(B.3)}$$
$$-\tau R_0^2\Big[ln(\frac{R^2}{R_0^2}) - \frac{(R_x^2-R_0^2)}{R_0^2}\Big]\Big\}.$$

At X-point, $B_z(R_x, Z_x) = 0$, which gives

$$Z_x = E\sqrt{\tau R_0^2 ln(\frac{R^2}{R_0^2}) + (2+\tau)(R_0^2 - R_x^2)}. \quad \text{(B.4)}$$

Toroidal magnetic field [to check]

$$B_\phi = \frac{B_0 R_0}{R}. \quad \text{(B.5)}$$

Around magnetic axis ($z \to 0$, $r \to R_0$), we can have

$$\psi = 4\psi_0\epsilon^2,\ \epsilon \equiv \frac{r-R_0}{R_0} \ll 1,\ \kappa \equiv \frac{2E}{\sqrt{1-R_x^2/R_0^2}}. \quad \text{(B.6)}$$

Thus poloidal magnetic field and safety factor around O-point is

$$B_p = 8\frac{\psi_0}{R_0^2}\epsilon,\ \ q_0 = \frac{rB_0}{R_0 B_p} = \frac{B_0 R_0^2}{8\psi_0}, \quad \text{(B.7)}$$

which gives

$$\psi_0 = \frac{B_0 R_0^2}{8q_0}. \quad \text{(B.8)}$$

The above model is very convenient to construct tokamak and spherical tokamak configurations.

To construct FRC configuration, we set $\tau = 0$, $R_x = 0$ and $B_\phi = 0$, which yields Hill-vortex equilibrium. And we set the magnetic $B_z(0,0) = B_0$, which gives $\psi_0 = \frac{B_0 R_0^2}{4}$. The FRC model also holds for mirror configuration, we only need set further $R_0^2 < 0$. That is, the Eq.(B.1) can combine all the above several configurations in one model.

We construct the density and temperature profiles as

$$n_{s0}(r,z) = n_{s00} e^{-\frac{\psi}{\psi_x L_{ns}^2}}, \tag{B.9}$$

$$T_{s0}(r,z) = T_{s00} e^{-\frac{\psi}{\psi_x L_{ts}^2}}, \tag{B.10}$$

where n_{s00} and T_{s00} are density and temperature of species s at O-point, and L_{ns} and L_{ts} are normalized scaling length of their radial profiles, with $\psi_x \equiv \psi(R_x, Z_x)$. Thus, the derivatives are readily obtained, say

$$\frac{\partial n_{s0}}{\partial r} = -\frac{1}{\psi_x L_{ns}^2} n_{s0}(r,z) \frac{\partial \psi}{\partial r} = -\frac{r B_z}{\psi_x L_{ns}^2} n_{s0}, \tag{B.11}$$

$$\frac{\partial n_{s0}}{\partial z} = -\frac{1}{\psi_x L_{ns}^2} n_{s0}(r,z) \frac{\partial \psi}{\partial z} = \frac{r B_r}{\psi_x L_{ns}^2} n_{s0}. \tag{B.12}$$

The derivatives of magnetic field components are also readily obtained, and not shown here.

References

[1] H.S. Xie, BO: A unified tool for plasma waves and instabilities analysis, Comput. Phys. Comm. 244 (2019) 343-371. Xie, H. S., Denton, R., Zhao, J. S. and Liu, W, BO 2.0: Plasma Wave and Instability Analysis with Enhanced Polarization Calculations arXiv:2103.16014, 2021.

[2] H.S. Xie, Y. Xiao, PDRK: A General Kinetic Dispersion Relation Solver for Magnetized Plasma, Plasma Sci. Technol. 18 (2) (2016) 97, http://dx.doi.org/10.1088/1009-0630/18/2/01, Update/bugs fixed at http://hsxie.me/codes/pdrk/ or https://github.com/hsxie/pdrk/.

[3] H. S. Xie, PDRF: A general dispersion relation solver for magnetized multi-fluid plasma, Comput. Phys. Comm. 185 (2014) 670-675.

[4] A.P. Smirnov and R.W. Harvey, The GENRAY Ray Tracing Code, 2003. https://www.compxco.com/Genray_manual.pdf. https://github.com/compxco/genray.

[5] Y. Peysson, J. Decker and L. Morini, A versatile ray-tracing code for studying rf wave propagation in toroidal magnetized plasmas, Plasma Physics and Controlled Fusion, 54 (2012) 045003.

[6] E. Mazzucato, I. Fidone and G. Granata, Damping of electron cyclotron waves in dense plasmas of a compact ignition tokamak, Physics of Fluids, 30 (1987) 3745-3751.

[7] D. B. Batchelor and R. C. Goldfinger, RAYS: a geometrical optics code for EBT, ORNL/TM-6844, 1982.

[8] M. Brambilla, Ray tracing of lower hybrid and ion cyclotron waves, Computer Physics Reports, 4 (1986) 71-93.

[9] A. Esterkin and A. Piliya, Fast ray tracing code for LHCD simulations, Nuclear Fusion, 36 (1996) 1501-1512.

[10] A. Fukuyama, Integrated Tokamak Code: TASK, version 5, 20180117, Kyoto University.

[11] B.D. McVey, A ray-tracing analysis of fast-wave heating of tokamaks, Nuclear Fusion, 19 (1979) 461.

[12] L. Lao, H. S. John, R. Stambaugh, A. Kellman and W. Pfeiffer, Reconstruction of current profile parameters and plasma shapes in tokamaks, Nuclear Fusion, 25 (1985) 1611.

[13] X. Yang, Y. Petrov, F. Ceccherini1, A. Koehn, L. Galeotti, S. Dettrick, M. Binderbauer and the TAE TeamSimulations of High Harmonic Fast Wave Heating on the C-2U Advanced Beam-Driven Field-Reversed Configuration Device, EPJ Web Conf. 157 (2017) 03065.

[14] H. J. Ma, H. S. Xie, B. H. Deng, Y. K. Bai, S. K. Cheng, Y. Li, B. Chen, M. Tuszewski, H. Y. Zhao and J.Y. Liu, A new tool GSEQ-FRC for two-dimensional field-reversed configuration equilibrium, Nuclear Fusion, (2021) https://doi.org/10.1088/1741-4326/ac0232.

[15] A. G. Shalashov, E. D. Gospodchikov, O. B. Smolyakova, P. A. Bagryansky, V. I. Malygin and M. Thumm, Auxiliary ECR heating system for the gas dynamic trap, Physics of Plasmas 19 (2012) 052503.

[16] J. C. Li, X. T. Ding, J. Q. Dong and S. F. Liu, Helicon wave heating and current drive in toroidal plasmas, Plasma Physics and Controlled Fusion 62 (2020) 095013.

[17] J. S. Zheng, G. H. Zhu, J. Y. Xiao and X. Sun, Three-dimensional structure-preserving electromagnetic particle-in-cell simulation of lower hybrid wave propagation and heating in the magnetic mirror, to be submitted, 2021.

[18] A. Ishida, Y. Martin Peng and W. J. Liu, Four-fluid axisymmetric plasma equilibrium model including relativistic electrons and computational method and results, Phys. Plasmas 28 (2021) 032503.

[19] T. Onchi, H. Idei, M. Fukuyama, D. Ogata, R. Ashida, T. Kariya, A. Ejiri, K. Matsuzaki, Y. Osawa, Y. Peng, S. Kojima, O. Watanabe, M. Hasegawa, K. Nakamura, K. Kuroda, R. Ikezoe, T. Ido, K. Hanada, N. Bertelli, M. Ono and A. Fukuyama, Non-inductive plasma current ramp-up through oblique injection of harmonic electron cyclotron waves on the QUEST spherical tokamak, Physics of Plasmas 28 (2021) 022505.

[20] Y. J. Shi, B. Liu, S. D. Song, Y. Y. Song, X. M. Song, B.W. Tong, S.K. Cheng, W.J. Liu, M.Y, Wang, T.T. Sun, D. Guo, S.J. Li, Y.Y. Li, B. Chen, X. Gu, J.Q. Cai, D. Luo, D. Banerjee, X. Zhao, Y.M. Yang, W.W. Luo, P. H. Zhou, Y. Wang, A. Ishida, T. Maekawa, M. S. Liu, B. S. Yuan, Y-K Martin Peng and the EXL-50 team, Solenoid-free current drive via ECRH in EXL-50 spherical torus plasmas, arXiv:2104.14844, 2021.

[21] M. Ono, N. Bertelli, H. Idei, K. Hanada, T. Onchi, S. Kojima, and H. Elserafy, Modeling of solenoid-free start-up using 2nd harmonic electron cyclotron heating and current drive in QUEST, AIP Conference Proceedings 2254 (2020) 090001.

[22] M. Liu, H. S. Yi, G. H. Zhu, Z. D. Yang, M.N. Lin, and X. Sun, Ion cyclotron resonant heating in the central cell of the Keda Mirror with AXisymmetricity KMAX, Physics of Plasmas 25 (2018) 082515.

[23] P. Helander and D. Sigmar, Collisional Transport in Magnetized Plasmas, Cambridge University Press, 2001, 292. Chapter 7.